Recycling the industrial waste $ZnFe_2O_4$ from hot-dip galvanization sludge

Fanni Fekete[1], László Péter Bakos[1], Károly Lázár[2], Anna Mária Keszler[3], Anna Jánosity[3], Li Zhibin[4], Imre Miklós Szilágyi[1,*] and László Kótai[3]

[1]Department of Inorganic and Analytical Chemistry, Budapest University of Technology and Economics, H-1111 Budapest, Szt. Gellért tér 4. Hungary

[2]Department of Nuclear Analysis and Radiography, Centre for Energy Research, Hungarian Academy of Sciences, H-1121 Budapest, Konkoly Thege M. út 29-33, Hungary

[3]Institute of Materials and Environmental Chemistry, Research Centre for Natural Sciences, Hungarian Academy of Sciences, H-1117 Budapest, Magyar tudósok körútja 2. Hungary

[4]Jiangmen XuHong Magnets Ltd, Xinsha Industrial Zone, Jiangmen City, China

Corresponding author: imre.szilagyi@mail.bme.hu

Keywords

$ZnFe_2O_4$, sludge, sulfation, TG/DTA-MS, XRD, FTIR, SEM, Mössbauer

Abstract

In this study, the goal was to find lower temperature for separating the Zn and Fe content of $ZnFe_2O_4$ by sulfation reaction than previously achieved, and to study the various reactions steps of sulfation. Hence, the reaction of $ZnFe_2O_4$ with Mohr's salt containing iron(II), i.e. $(NH_4)_2Fe(SO_4)_2 \cdot 6H_2O$, and ammonium iron alum containing Fe(III), i.e. $NH_4Fe(SO_4)_2 \cdot 12H_2O$ was studied. At first the thermal decomposition of precursor salts in air was studied by TG/DTA-MS to find the proper temperature for sulfation. Then $ZnFe_2SO_4$:precursor salt mixtures with ratios 1:2 and 1:5 were prepared and annealed at 400, 425, 450 °C. The solubility of the products obtained at different annealing temperatures in water (e.g. $ZnSO_4$, $FeSO_4$, $Fe_2(SO_4)_3$) and in HCl (Fe_2O_3, ZnO, $Fe_x(OH)_ySO_4$, $Zn_v(OH)_wSO_4$ basic sulfates) was studied. The morphology and structure of the starting materials was investigated by SEM, XRD and FTIR, the crystalline phases after each annealing and washing steps were studied by XRD. The Fe in the starting materials and the products obtained at 425 °C was measured by Mössbauer. Based on the obtained results,

it was demonstrated that the sulfation reaction with ammonium iron sulfates could be performed at lower temperatures than with iron sulfates. It was possible to detect the reaction intermediates and to obtain information about the reaction intermediates. With our sulfation reaction, depending on the reaction conditions, it is possible to obtain Fe_2O_3 as final product, but the Zn and Fe metals can be obtained also as sulfates. Our results open up further possibilities to recycle the $ZnFe_2O_4$ waste material.

1. Introduction

To protect iron products from corrosion, a zinc coating on iron is often used. Zn is usually deposited by hot dip galvanization (dipping into melted Zn) [1]. Before this, the iron surface is etched with an acidic solution to remove Fe_2O_3 and to deposit the first layer of Zn. This process results in the hot dip galvanization sludge, which contains e.g. $Fe(OH)_3$, $Fe(OH)_2$, FeO(OH), Fe_3O_4, $(Zn,Fe)Fe_2O_4$, $Zn(OH)_2$, $Zn_5(OH)_8Cl_2{\cdot}5H_2O$ etc. The sludge has 35 % dry content, and it can be stored only as a dangerous waste deposit. The sludge cannot be directly recycled in steel industry, due to its zinc content, because the zinc compounds are easily reduced into metallic zinc, which can destroy the wall of the blast furnace [2-4]. In order to recycle it, its Zn and Fe content has to be separated. After several annealing, washing and filtration steps, $ZnFe_2O_4$ can be isolated, and it will incorporate all the Fe content of the sludge.

Zn and Fe can be separated in several ways from $ZnFe_2O_4$: (a) dissolving in hot cc. H_2SO_4; (b) reacting with SO_2 and SO_3 in the presence of O_2; (c) reacting with in situ released SO_2 and SO_3, which form during annealing hydrated Fe(II) and Fe(III) sulfates or ammonium sulfates. These latter reactions can be easily performed with complete decomposition of zinc ferrite and with the formation of $Fe_2(SO_4)_3$ at 590 °C and Fe_2O_3 at 650 °C, respectively [6-13]. Since sulfation of zinc ferrite with ammonium, iron(II) or iron(III) sulfates operates around the softening point of black steel (600 °C), we turned huge efforts to find new and cheap sulfation agents, which have high enough SO_3 dissociation pressure to sulfate zinc ferrite at lower temperatures than 600 °C.

Accordingly, our aim was to find a way to lower the reaction temperature of sulfation. Furthermore, the various reactions steps of sulfation were also studied in detail. For the sulfation, ammonium-iron-sulfate precursors were used: Mohr's salt containing iron(II), i.e. $(NH_4)_2Fe(SO_4)_2{\cdot}6H_2O$, and ammonium iron alum containing iron(III), i.e. $NH_4Fe(SO_4)_2{\cdot}12H_2O$.

At first the thermal decomposition of precursor salts in air was studied by TG/DTA-MS to find the proper temperature for sulfation. The use of evolved gas analysis (EGA) in this was essential, since EGA provides useful information about the release of gaseous species during the thermal decomposition of various substances [14-23]. Then $ZnFe_2SO_4$:precursor salt mixtures with ratios 1:2 and 1:5 were prepared

and annealed at 400, 425, 450 °C. To study the water (e.g. $ZnSO_4$, $FeSO_4$, $Fe_2(SO_4)_3$) and acid (Fe_2O_3, ZnO, $Fe_x(OH)_ySO_4$, $Zn_v(OH)_wSO_4$ basic sulfates) soluble constituents, the as-annealed products were washed with water and HCl. The morphology and structure of the starting materials was investigated by SEM, XRD and FTIR, the crystalline phases after each annealing and washing steps were studied by XRD, and the Fe in the starting materials and the products obtained at 425 °C was measured by Mössbauer.

2. Experimental

$ZnFe_2O_4$ was prepared by annealing 50-50 mol% mixture of Fe_2O_3 and ZnO (1000 °C, 4 h), then washed with H_2O and HCl. Mohr's salt (iron(II)), $(NH_4)_2Fe(SO_4)_2{\cdot}6H_2O$ was synthesized by reacting $FeSO_4$ (dissolved in H_2SO_4) and $(NH_4)_2SO_4$ in 1:1 ratio. Ammonium iron(III) alum, $NH_4Fe(SO_4)_2{\cdot}12H_2O$ was obtained by reacting aqueous $Fe_2(SO_4)_3$ and $(NH_4)_2SO_4$ in 1:1 ratio. For preparing the 1:2 $ZnFe_2O_4$:ammonium iron sulfate reaction mixtures, 1 g mixture batches were grinded in a mortar, then annealed and washed with H_2O. For preparing the 1:5 $ZnFe_2O_4$:ammonium iron sulfate reaction mixtures, 30-40 g mixture batches were grinded in a ball mill, then annealed and washed with H_2O and HCl. Only 2 h reaction time was used for the mixtures in order not to reach complete conversion and therefore to enable to study the reaction intermediates and the reaction mechanisms.

SEM images were recorded by a JEOL JSM-5500LV scanning electron microscope.

Powder XRD patterns were measured on a PANalytical X'pert Pro MPD X-ray diffractometer using Cu K_α radiation.

FTIR spectra were obtained by an Excalibur Series FTS 3000 (Biorad) FTIR spectrophotometer in the range of 400-4000 cm^{-1} in KBr pellets.

The thermal decomposition of the samples was studied by a TG/DTA-MS apparatus, which consisted of an STD 2960 Simultaneous TGA/DTA (TA Instruments Inc.) thermal analyzer and a Thermostar GSD 200 (Balzers Instruments) quadrupole mass spectrometer. On-line coupling between the two parts was provided through a heated (T = 200°C) 1 m 100% methyl deactivated fused silica capillary tube with inner diameter of 0.15 mm. A mass/charge range between m/z = 1 – 200 was monitored by scan mode. During the measurements an open platinum crucible, a heating rate of 10 °C min^{-1}, sample sizes of 5 – 6 mg and flowing air (130 ml min^{-1}) were used.

3. Results and discussion

3.1. Properties of the starting materials

Based on XRD (Fig. 1) and FTIR [24-26] (Fig. 2) patterns, the as-synthesized $ZnFe_2O_4$ (PDF 04-006-8036), $(NH_4)_2Fe(SO_4)_2{\cdot}6H_2O$ (PDF 04-010-5616), $NH_4Fe(SO_4)_2{\cdot}12H_2O$ (PDF 04-009-6221) were pure and they did not contain any impurities. Their morphology was studied by SEM (Fig. 3), and their particle sizes were in the range of 60-150µm, 60-80 µm with larger aggregates, and above 200 µm with aggregates, respectively.

3.2. Thermal behavior of the Mohr's salt, $(NH_4)_2Fe(SO_4)_2{\cdot}6H_2O$ starting material

The thermal decomposition of $(NH_4)_2Fe(SO_4)_2{\cdot}6H_2O$ in the air was already studied previously [27] with TG and Mössbauer methods. It was stated that the salt decomposed in a multistep decomposition process with stepwise dehydration and ammonia loss with the formation of various iron(III) intermediates, including anhydrous iron(III) sulfate ($Fe_2(SO_4)_3$) at 450 °C, and Fe_2O_3 at 730 °C as final product.

Our thermal analysis (TG/DTA-MS) data of $(NH_4)_2Fe(SO_4)_2{\cdot}6H_2O$ in air atmosphere are presented in Fig. 4 and Table 1. Between 90-250 °C in three overlapping reactions, 2-2-2 crystal waters were released (17^+, 18^+) with a mass loss of 28 %.

In the second main decomposition process (250-350 °C) ammonia (15^+, 16^+, 17^+) was released and its oxidation products (30^+, 46^+) in air were also observed. From 310 °C the evolution of SO_2/SO_3 was also detected. The evolution of nitrogen (discussed later) could not be monitored due to the usage of air atmosphere, which contains elementary N_2. Since synthetic air beside 20 % oxygen contains 80 % nitrogen, and the sensitivity of the measurement was not high enough to detect the nitrogen evolution. The mass loss of 4.4 % corresponds to the release of 1 NH_3 together with a small amount of SO_2/SO_3. The DTA curve had an endothermic peak as well here.

Frank described an unidentified iron(III)-containing phase formed during decomposition of Mohr's salt with a singlet Mössbauer peak (IS=0.7 mm/s) [27]. Delgado-Lopez found the formation of $NH_4Fe(SO_4)_2$ from a double salt $(NH_4)_2SO_4{\cdot}Fe_2(SO_4)_3$ under heating [28]. This double salt has the same chemical constitution as the anhydrous ammonium iron(III) alum. The process is endothermic similar to the peak found by us at 317 C°. According to Fig. 4, in the temperature range to about 200 °C reaction (1) is taking place, followed by reaction (2) with the endothermic peak at 317 °C.

$$2(NH_4)_2Fe(SO_4)_2 + 1/2O_2 = H_2O + (NH_4)_2SO_4{\cdot}Fe_2(SO_4)_3 + 2NH_3 \quad (1)$$

and

$3(NH_4)_2SO_4 \cdot Fe_2(SO_4)_3 = 3Fe_2(SO_4)_3 + 3H_2O + 4NH_3 + N_2 + 3SO_2$ (2)

Delgado-Lopez found that this compound was completely transformed around 300 °C with appearance of ammonium iron(III) alum [28]. Nakamura [29] has defined a redox reaction of $NH_4Fe(SO_4)_2$ proceeding in an analogous way according to the next equation (3):

$6\ NH_4Fe(SO_4)_2 = 3Fe_2(SO_4)_3 + 6H_2O + 4\ NH_3 + N_2 + 3SO_2$ (3)

In their study, the reaction was completed between 370 and 444 °C, i.e. the alum is formed below 350 °C from the double salt; thus, in our case the decomposition of the double salt with the same stoichiometric components could be observed at 317 °C. Taking into consideration these results, the iron(III) containing phase with IS=0.7 without splitting might be the double salt $(NH_4)_2SO_4 \cdot Fe_2(SO_4)_3$ formed as precursor of the redox reaction observed around 300 °C, and a relationship is supposed between the appearance of this phase and the observed redox reaction [29].

In the third decomposition process (350-500 °C) mostly SO_2 and SO_3 evolved (48^+, 64^+, 80^+) in an endothermic reaction, and their release was the most intense at 460 °C. Beside them, some oxidation products of as-released NH_3 were also observed [30].

The fourth decomposition process took place at 500-750 °C, and here again SO_2 and SO_3 evolved together with small amounts of NH_3. The residual mass of 21.2 % corresponds to 0.5 mol Fe_2O_3, which formed through the release of SO_3. The XRD analysis of the final residue also detected only this phase (PDF 00-021-0920).

The decomposition of SO_3 into SO_2 and O_2 in the third and fourth steps was supressed at this temperature due to the presence of aerial oxygen; therefore, SO_2 and SO were detected only as fragments of SO_3 during the electron impact ionization in the mass spectrometer, which is confirmed by the same shapes of the SO_3/SO_2/SO fragment ions.

3.3. Thermal behavior of the ammonium iron alum, $(NH_4)_2Fe_2(SO_4)_2 \cdot 12H_2O$ starting material

The thermal decomposition of ammonium iron alum was also studied previously [28-29,31]. Our TG/DTA-MS curves of $(NH_4)_2Fe_2(SO_4)_2 \cdot 12H_2O$ in air atmosphere are shown in Fig. 5 and Table 1. The general character of the decomposition recorded by us agrees with the previous results.

Until 200 °C in overlapping endothermic reactions the crystal water content is released and water free $(NH_4)_2Fe(SO_4)_2$ is formed. From here the decomposition sequences of $(NH_4)_2Fe_2(SO_4)_2 \cdot 12H_2O$ and $(NH_4)_2Fe(SO_4)_2 \cdot 6H_2O$ are similar. The nature of gas-phase components is also almost the same as in case of Mohr's salt. It can be easily explained because in the air, in the case of the decomposition process of the Mohr's salt at the beginning the same intermediates appear as during the decomposition of the ammonium iron(III) alum.

Nakamura defined a redox reaction between the sulfate and ammonia, with N_2 formation, which is formally an analog of the reaction found in case of Mohr's salt (3) and the two processes take place at the same temperature (DTA peak temperature was found by us to be 317 °C in both cases) (4) [29].

It is supposed that the ammonia is oxidized into N_2 by the sulfater content of the salt, without reduction of iron(III) into iron(II). At the same temperature where the Mohr's salt was decomposed (peak 317 °C), a redox reaction takes place, which is formally almost the same as we found in case of Mohr's salt.

In the third decomposition process (350-550 °C), mostly SO_2 and SO_3 were released together with a small amount of NH_3 and its oxidation products. The evolution of SO_2 and SO_3 was the most intense at 455 °C. The first SO_2 peak appears without SO_3 signal; thus, the source of SO_2 might be sulfuric acid as well. The SO_2 and SO_3 evolution peaks in the MS ion current curves are around 455 °C, which is only a bit lower than in the case of $(NH_4)_2Fe(SO_4)_2 \cdot 6H_2O$.

In the fourth, final decomposition step (500-700 °C) the release of sulfur oxides continued. The final product (25 mass%) was Fe_2O_3, which was also confirmed by XRD.

3.4. Results with 1:2 $ZnFe_2O_4$:ammonium iron sulfate reaction mixtures

In the gas phase there is an equilibrium between SO_2 and SO_3, which supplements the used SO_3 (it is SO_3, which makes the sulfation reaction with $ZnFe_2O_4$). The release of sulfur oxides took place in two temperature regions from the samples, i.e. 350-500 and 500-750 °C. For the sulfation reaction, the lower temperature region sulfur oxide release was selected, since it required less energy and hence it was more economic. We considered that if the SO_3 evolution from the precursors is too intensive (at and above 450-460 °C), this reagent might run out too fast. However, our aim was to study the reaction mechanism as well. Thus, the sulfation reaction temperatures were selected in the temperature region before the maximum SO_2 and SO_3 evolution peaks, i.e. at 400-425-450°C.

In order to determine the decomposition mechanism, the composition of the samples isolated at 400, 425 and 450 °C from the 1:2 mixtures of $ZnFe_2O_4$ with $(NH_4)_2Fe(SO_4)_2 \cdot 6H_2O$ or $NH_4Fe(SO_4)_2 \cdot 12H_2O$ (Table 2) were analyzed by XRD measurements(Fig. 6). The XRD pattern showed $Fe_2(SO_4)_3$ (PDF 04-033-0679), Fe_2O_3 (PDF 00-021-0920), and $ZnFe_2O_4$ (PDF 04-015-7055) crystalline phases. The presence of ZnO or $ZnSO_4$ was also supposed; however, they might have been present in amorphous form.

When the as-prepared samples were washed with water, bubbling was observed, which was explained by the release of gases trapped during the sulfation reaction in the solid samples. Some of the released sulfur oxides formed sulfur acids (e.g. H_2SO_4 and H_2SO_3 from SO_3 and SO_2), which was an exothermic reaction in water and thus the solution warmed up.

3.5. Results with 1:5 $ZnFe_2O_4$:ammonium iron sulfate reaction mixtures

To study the influence of different amounts of the reagents, the ratio of the starting materials was modified to 1:5. In addition, beside washing with water, a washing step also with HCl was included to further study reaction intermediates, and the sample batch masses were increased to have enough sample to the studies. The yield of the 1:5 $ZnFe_2O_4$:ammonium iron sulfate reaction mixtures and the masses after H_2O and HCl washing steps can be seen in Table 3.

Based on XRD data (Fig. 7), when $ZnFe_2O_4$ was reacted with Mohr's salt in 1:5 ratio, in the product at 400 °C (VII) $ZnFe_2O_4$, $Fe_2(SO_4)_3$, $NH_4Fe(SO_4)_2$ could be detected as crystalline phases, at 425 °C (VIII) $ZnFe_2O_4$, $Fe_2(SO_4)_3$, $NH_4Fe(SO_4)_2$, $Fe_{5,34}O_3(SO_4)_{5,01}$, and at 450 °C (IX) $Fe_2(SO_4)_3$, $ZnFe_2O_4$. Similarly, when $ZnFe_2O_4$ was reacted with ammonium iron alum in 1:5 ratio, in the product at 400 °C (X) $ZnFe_2O_4$, $Fe_2(SO_4)_3$, $Fe_4(OH)_{10}SO_4$ could be observed as crystalline phases, at 425 °C (XI) $ZnFe_2O_4$, $Fe_2(SO_4)_3$, $Fe_4(OH)_{10}SO_4$, and at 450 °C (XII) $Fe_2(SO_4)_3$, $ZnFe_2O_4$. The Zn phases could be present here also in amorphous form.

When the as-prepared samples were washed with H_2O (Fig. 8), all sulfates were removed. Only $ZnFe_2O_4$ remained in the samples, plus some FeO(OH) compounds. Finally, when these samples were washed further with HCl (Fig. 9), only $ZnFe_2O_4$ remained in the samples. In the case of samples VII (1:5 $ZnFe_2O_4$:Mohr's salt at 400 °C), VIII (1:5 $ZnFe_2O_4$:Mohr's salt at 425 °C), and X (1:5 $ZnFe_2O_4$:ammonium iron alum at 400 °C) a colloid precipitate formed after H_2O washing, which dissolved after HCl washing. This already in itself suggests the formation of basic iron sulfate-hydroxides.

3.6. Mössbauer study of the sulfation reaction

Fig. 10a-c contains the Mössbauer spectra of $(NH_4)_2Fe(SO_4)_2 \cdot 6H_2O$, $NH_4Fe(SO_4)_2 \cdot 12H_2O$, and $ZnFe_2O_4$ starting materials, respectively. The measured values (IS/ mm s^{-1}: 1.25, QS/ mm s^{-1}: 1.72 for $(NH_4)_2Fe(SO_4)_2 \cdot 6H_2O$; IS: 0.465 for $NH_4Fe(SO_4)_2 \cdot 12H_2O$; and IS: 0.346, QS: 0.432 for $ZnFe_2O_4$) corresponded to literature data [25,32-33].

Samples VIII (1:5 mixture of $ZnFe_2O_4$ and $(NH_4)_2Fe(SO_4)_2 \cdot 6H_2O$ annealed 425 °C) and XI (1:5 mixture of $ZnFe_2O_4$ and $NH_4Fe(SO_4)_2 \cdot 12H_2O$ annealed at 425 °C) had a large singlet and small doublet in their Mössbauer spectra, which corresponded to mostly $Fe_2(SO_4)_3$ and small amount of $ZnFe_2O_4$ (Fig. 10d-e) [34-35]. Thus, according to Mössbauer spectra (Fig. 10), the Fe component of $ZnFe_2O_4$ transformed mostly to $Fe_2(SO_4)_3$.

3.7. Reaction of $ZnFe_2O_4$ with Mohr's salt, $(NH_4)_2Fe(SO_4)_2 \cdot 6H_2O$

It has to be remarked that in the low-temperature SO_3 evolution range only the ¼ part of the sulfation capacity of Mohr's salt can be utilized compared to the high-temperature process. The XRD and Mössbauer studies of the formed and water-leached residues did not show the presence of considerable amount of Fe_2O_3 at all, neither from the Mohr's salt decomposition nor from the zinc ferrite sulfation. The main iron-containing product obtained was $Fe_2(SO_4)_3$ (confirmed by Mössbauer and XRD); thus, the sulfation product of zinc ferrite in this temperature range with Mohr's salt proved to be $ZnSO_4$ and $Fe_2(SO_4)_3$. It shows that Mohr's salt can sulfate the iron content of the zinc ferrite into $Fe_2(SO_4)_3$, since Fe_2O_3 transforms in this temperature range into $Fe_2(SO_4)_3$ in the presence of an SO_3 source like ammonium sulfate [9]. According to this, the stoichiometry of the process requires much more Mohr's salt as that could be supposed based on the formation of Fe_2O_3 from the ferrite or Mohr's salt in the high-temperature process. Hence, in the case of annealing the $ZnFe_2O_4$:Mohr's salt=1:5 ratio mixture at 425 °C for 2 h, the presence of unreacted $ZnFe_2O_4$ could be confirmed by Mössbauer and XRD as well. According to the equation (4), at least 1:8 $ZnFe_2O_4$:Mohr's salt ratio has to be used to complete the sulfating of zinc ferrite,

$$ZnFe_2O_4 + 8\,(NH_4)_2Fe(SO_4)_2 + 2O_2 = ZnSO_4 + 8H_2O + 5Fe_2(SO_4)_3 + 16NH_3 \qquad (4)$$

It means that in practice due to by-reactions, even more, ~10-fold excess of Mohr's salt should be used to complete the sulfation of zinc ferrite at this temperature range.

3.8. Reaction of $ZnFe_2O_4$ with ammonium iron alum, $(NH_4)_2Fe_2(SO_4)_2 \cdot 12H_2O$

The sulfation process (5) can be written with the same $Zn:SO_4^{2-}$ stoichiometry as in the case of Mohr's salt.

$$ZnFe_2O_4 + 8\ NH_4Fe(SO_4)_2 = ZnSO_4 + 5Fe_2(SO_4)_3 + 8NH_3 + 4H_2O \quad (5)$$

In this process, the ¼ part of the sulfate content of the ammonium iron(III) alum turns into SO_3 in the zinc ferrite sulfation process. According to this, the 1:8 molar ratio is the minimal $ZnFe_2O_4$:alum molar ratio. Therefore, the Mössbauer of the $ZnFe_2O_4$:$NH_4Fe(SO_4)_2 \cdot 12H_2O$ reaction mixture heated at 425 °C for 2 h showed the presence of some amount of residual zinc ferrite and the signal of the undecomposed anhydrous ammonium iron(III) sulfate [26].

Separation of $ZnSO_4$ from the as-obtained $Fe_2(SO_4)_3$ can easily be performed with e.g. the formation of Fe_2O_3 by high temperature (200 °C) hydrolysis using aqueous sulphuric acid developed by Umetsu et al [26]. Based on them, although the hydrolysis of $Fe_2(SO_4)_3$ results $Fe(OH)SO_4$ instead of Fe_2O_3 above 60 g/L sulfuric acid concentration, in the presence of zinc sulfate, this acid concentration could be increased until almost 10 %. The phase diagrams for various sulfuric acid (formed in the hydrolysis reaction) and zinc sulfate concentrations have been presented previously [26].

4. Conclusion

In this study, the goal was to find lower temperature for separating the Zn and Fe content of $ZnFe_2O_4$ by sulfation reaction than previously achieved, and to study the various reactions steps of sulfation. Hence, we studied the reaction of $ZnFe_2O_4$ with Mohr's salt containing iron(II), i.e. $(NH_4)_2Fe(SO_4)_2 \cdot 6H_2O$, and ammonium iron alum containing Fe(III), i.e. $NH_4Fe(SO_4)_2 \cdot 12H_2O$ at 400-425-450 °C. These temperatures were selected since these are below the maximum release temperature of sulfur oxides from Mohr's salt and ammonium iron alum, and thus it gave us chance to study the reaction intermediates and hence the reaction mechanisms.

Based on the obtained results, at each temperature the Fe content transformed mostly to $Fe_2(SO_4)_3$, which partly hydrolysed and could be isolated as a colloid precipitate, FeO(OH) by washing with water and HCl. At lower temperatures (400-425 °C for Mohr's salt and 400 °C for ammonium iron alum) the presence of basic iron-sulfate was also suggested. This basic iron sulfate formed also colloid precipitate by dissolution by water and could be isolated as iron hydroxide or iron oxide hydroxide.

The Zn content of $ZnFe_2O_4$ transformed into similar amounts of amorphous $ZnSO_4$ and basic Zn-sulfate-hydroxides. Since $ZnSO_4$ is stable until 680°C, the basic Zn-sulfate-hydroxide might be its intermediate. It was found that the stoichiometry of the annealing reaction was influenced by the temperature and by the reactant ratios. With 2 h reaction time, the yield was 52-78% at 425 °C (Table 3). Our results open up further possibilities to recycle the $ZnFe_2O_4$ waste material. E.g. by applying longer annealing at 400-450 °C or heat shock at 600-650 °C, it might be possible to convert all Fe content of $ZnFe_2O_4$ to Fe_2O_3. Here zinc sulfate is still thermally stable and can be washed out by water. Another option is that $Fe_2(SO_4)_3$ and $ZnSO_4$ can be obtained separately after fractional crystallization. Thus, harmful gas release can be reduced this way (S will be bonded in the form of SO_4^{2-}). Finally, when reacting $ZnFe_2O_4$ with $(NH_4)_2SO_4$, the product $Fe_2(SO_4)$ can be transformed back into $NH_4Fe(SO_4)_2 \cdot 12H_2O$, and can be reused in this reaction, or can be used for other purposes (e.g. wastewater cleaning).

To conclude, it was demonstrated that the sulfation reaction with ammonium iron sulfates could be performed at lower temperatures than with iron sulfates. It was possible to detect the reaction intermediates and to obtain information about the reaction intermediates. With our sulfation reaction, depending on the reaction conditions, it is possible to obtain Fe_2O_3 as final product, but the Zn and Fe metals can be obtained also as sulfates.

5. Acknowledgements

I. M. Szilágyi acknowledges a János Bolyai Research Fellowship of the Hungarian Academy of Sciences and an ÚNKP-18-4-BME-238 grant supported by the New National Excellence Program of the Ministry of Human Capacities, Hungary. An NRDI K 124212 and an NRDI TNN_16 123631 grant are acknowledged. The research within project No. VEKOP-2.3.2-16-2017-00013 and GINOP-2.2.1-15-2017-00084 was supported by the European Union and the State of Hungary, co-financed by the European Regional Development Fund. The research reported in this paper was supported by the Higher Education Excellence Program of the Ministry of Human Capacities in the frame of Nanotechnology and Materials Science research area of Budapest University of Technology (BME FIKP-NAT).

6. References

[1] General galvanizing paractice. Hot Dip Galvanizers Associacion, London, 1965.

[2] Kazinczy B, Kótai L, Gács I, Szentmihályi K, Sándor Z, Holly S. Study on ammoniacal leaching of zinc from sludges containing iron and zinc hydroxides. Hung. J. Ind. Chem. 2000;28:207-10.

[3] Arsenovic M, Radojevic Z, Stankovic S. Removal of toxic metals from industrial sludge by fixing in brick structure. Const. Build. Mater. 2012;37:7-14.

[4] Yakornov SA, Grudinsky PI, Dyubanov VG, Leont'ev LI, Kozlov PA, Ivakin D A. Thermodynamic analysis of zinc ferrite decomposition in electric arc furnace dust by lime. Russ. J. Non-Ferr. Met. 2017;58:586-90.

[5] Junca E, Grillo FF, Restivo TAG, de Oliveira JR, Espinosa DCR, Tenório JAS. Kinetic investigation of synthetic zinc ferrite reduction by hydrogen, J. Therm. Anal. Calorim. 2017;129:1215-23.

[6] Kazinczy B, Kótai L, Sajó IE, Holly S, Lázár K, Jakab E, Gács I, Szentmihályi K. Phase relations and heat-induced chemical processes in sludges os Hot-dip galvanization. Ind. Eng. Chem. Res. 2002;41:720-5.

[7] Kazinczy B, Kótai L, Gács I, Sajó IE, Sreedhar B, Lázár K. Study of the preparation of zinc(II)zerrite and ZnO from zinc- and iron-containing industrial wastes. Ind. Eng. Chem. Res. 2003;42:318-22.

[8] Saini A, Kótai L, Sajó IE, Szilágyi IM, Lázár K, May Z, Fazekas P, Gács I, Sharma V, Banerji KK. Solid phase sulphatizing of znc-ferrite spinel with iron sulphates as an environmental friendly way for recovering zinc. Eur. Chem. Bull. 2012;1:7-13

[9] Nagaishi T, Ishiyama S, Matsumoto M, Yoshinaga S. Reactions between ammonium-sulphate and metal oxides (Cr,Mn,Fe) and thermal decomposition of the products. J. Therm. Anal. 1984;29:121-9.

[10] Mohai I, Szépvölgyi J, Bertóti I, Mohai M, Gubicza J, Ungár T. Thermal plasma synthesis of zinc ferrite nanopowders. Solid State Ionics 2001;163:141-2.

[11] Mohai I, Szépvölgyi J, Károly Z, Mohai M, Babijevszkaja IZ, Krenev VA. Reduction of metallurgical wastes in an RF thermal plasma reactor. Plasma Chem. Plasma Process. 2001;21:547.

[12] Boyanov BS. Interaction of $(NH_4)_2SO_4$ and $FeSO_4$ with metal oxides and ferrites. Thermochim. Acta 1994;240:225.

[13] Jiang GM, Peng B, Liang YJ, Chai LY, Wang QW, Li QZ, Hu M. Recovery of valuable metals from zinc leaching residue by sulfate roasting and water leaching. Trans. Nonferr. Met. Soc. Chin. (Eng. Ed.) 2017;27:1180-7.

[14] Pinto BV, Ferreira APG, Cavalheiro ETG. A mechanism proposal for fluoxetine thermal decomposition. J. Therm. Anal. Calorim. 2017;130:1553-1559.

[15] Opuchovic O, Niznansky D, Kareiva A. Thermoanalytical (TG/DSC/EVG-GC-MS) characterization of the lanthanide (Ho) iron garnet formation in sol-gel. J. Therm. Anal. Calorim. 2017;1085-1094.

[16] Krishnan GS, Murali N, Ahamed AJ. Structural transformation, thermal endurance, and identification of evolved gases during heat treatment processes of carbon fiber polymer precursors focusing on the stereoregularity. J. Therm. Anal. Calorim. 2017;130:1553-1559.

[17] Podkoscielna B, Sobiesiak M. Characteristics of thermal behavior of photoluminescent copolymers studied by the TG/DTG/FTIR coupled method. J. Therm. Anal. Calorim. 2016;125:625-631.

[18] Rogulska M, Kultys A. J. Aliphatic polycarbonate-based thermoplastic polyurethane elastomers containing diphenyl sulfide units. Therm. Anal. Calorim. 2016;126:225-243.

[19] Diyuk VE, Mariychuk RT, Lisnyak VV. Barothermal preparation and characterization of micro-mesoporous activated carbons Textural studies, thermal destruction and evolved gas analysis with TG-TPD-IR technique. J. Therm. Anal. Calorim. 2016;124:1119-1130.

[20] Bartyzel A, Sztanke M, Sztanke K. Thermal studies of analgesic active 8-aryl-2,6,7,8-tetrahydroimidazo[2,1-c][1,2,4]triazine-3,4-diones. J. Therm. Anal. Calorim. 2016;123:2053-2060.

[21] Ambrozini B, Cervini P, Cavalheiro ETG. Thermal behavior of the beta-blocker propranolol. J. Therm. Anal. Calorim. 2016;123:1013-1017.

[22] Papadopoulos C, Cristovao B, Ferenc W, Hatzidimitriou A, Vecchio Ciprioti S, Risoluti R, Lalia-Kantouri M. Thermoanalytical, magnetic and structural investigation of neutral Co(II) complexes with 2,2'-dipyridylamine and salicylaldehydes. J. Therm. Anal. Calorim. 2016;123:717-729.

[23] Mihaiu S, Szilagyi IM, Atkinson I, Mocioiu OC, Hunyadi D, Pandele-Cusu J, Toader A, Munteanu C, Boyadjiev S, Madarasz J, Pokol G, Zaharescu M. Thermal study on the synthesis of the doped ZnO to be used in TCO films. J. Therm. Anal. Calorim. 2016;124:71-80.

[24] Liu L, Zhang G, Wang L, Huang T, Qin L. Highly active S-modified $ZnFe_2O_4$ heterogeneous catalyst and its photo-fenton behavior under UV-Visible irradiation. Ind· Eng. Chem· Res· 2011;50:7219-27.

[25] Nyquist RA, Kagel RO. Infrared spectra of inorganic compounds. Acedemic Press New York and London, 1971.

[26] Music S, Saric A, Popovic S, Nomura K, Sawada T. Forced hydrolisis of Fe^{3+} ions in $NH_4Fe(SO_4)_2$ solutions containing Urotropine. Croat. Chem. Acta 2000;73:541-67.

[27] Frank E, Varriale MC, Bristotti A. Mössbauer studies of the thermal decomposition of iron(II) ammonium sulphate hexahydrate. J. Therm. Anal. 1979;17:141-50.

[28] Lopez-Delgado A, Lopez FA. Thermal decomposition of ferric and ammonium sulfates obtained by bio-oxidation of water pickling liquors with Thiobacillus ferrooxidans. J. Mater. Sci. 1995;30:5130-8.

[29] Nakamura H, Hara Y, Osada H, The thermal decomposition of ammonium sulfate and its reaction with iron(III) oxide. Nippon Kagaku Kaishi 1980;5:706-710.

[30] Kocsis T, Magyari J, Sajó IE, Pasinszki T, Homonnay Z, Szilágyi IM, Farkas A, May Z, Effenberger H, Szakáll S, Pawar RP, Kótai K. Evidence of quasi-intramolecular redox reactions during thermal decomposition of ammonium hydroxodisulphitoferriate(III), $(NH_4)_2[Fe(OH)(SO_3)_2]\cdot H_2O$. J. Therm. Anal. Calorim. 2018;132:493-502.

[31] Oliviera AC, Garg VK. Mössbauer aqueous frozen solution and thermal decomposititon studies of $Fe(NH_4SO_4)_2\cdot 6H_2O$. Radiochem. Radioanal. Lett. 1974;18:43-8.

[32] Kopcewicz K, Kotlicji A, Szefer M. Mössbauer study of proton irradiation effects in hydrated iron(II) ammoniumm sulfate and iron (III) ammonium aluminate. Physica Status Solidi 1975;14:4159.

[33] Housley RM. Investigation of Magnetic Relaxation Effects in $Fe(NO_3)_3\cdot 9H_2O$ and $NH_4Fe(SO_4)_2\cdot 12H_2O$ by Mössbauer-Effect Sectroscopy. J. Appl. Phys. 1967;38:1287-9.

[34] Zboril R, Mashlan M, Petridis D, Krausova D, Pikal P. The role of intermediates in the process of red ferric pigment manufacture from $FeSO_4\cdot 7H_2O$. Hyperfine Interact. 2002;139/140:437-45.

[35] Pelovski Y, Petkova V, Nikolov S. Study of the mechanisam of the thermochemical decomposition of ferrous sulphate monohydrate. Thermochim. Acta 1996;274:273-80.

[36] Umetsu Y, Tozawa K, Sasaki K. The hydrolysis of ferric sulphate solutions at elevated temperatures. Can. Metall. Quart. 1977;116:111-7.

Tables

Table 1. Gaseous products detected by MS during the annealing of Mohr's salt and ammonium iron alum

m/z	Possible fragment
15^+	NH^+
16^+	NH_2^+; O^+
17^+	NH_3^+; OH^+
18^+	H_2O^+
30^+	NO^+
32^+	O_2^+
46^+	NO_2^+
48^+	SO^+
64^+	SO_2^+
80^+	SO_3^+

Table 2. Masses after anealing and H_2O washing step of 1:2 $ZnFe_2O_4$:ammonium iron sulfate reaction mixtures

Sample name	Reactants	Ratio	T/ °C	Mass% after annealing	Mass% dissolved in H_2O
I.	$ZnFe_2O_4$: Mohr's salt	1:2	400	66.97	84.87
II.	$ZnFe_2O_4$: Mohr's salt	1:2	425	66.04	92.14
III.	$ZnFe_2O_4$: Mohr's salt	1:2	450	65.32	75.22
IV.	$ZnFe_2O_4$: Amm-Fe(III) salt	1:2	400	62.87	89.51
V.	$ZnFe_2O_4$: Amm-Fe(III) salt	1:2	425	63.30	92.27
VI.	$ZnFe_2O_4$: Amm-Fe(III) salt	1:2	450	66.79	90.75

Table 3. Masses H_2O and HCl washing step and yield of 1:5 $ZnFe_2O_4$:ammonium iron sulfate reaction mixtures

Sample name	Reactants	Ratio	T/ °C	Mass% after H_2O and HCl washing	Yield
VII.	$ZnFe_2O_4$: Mohr's salt	1:5	400	47.38	52.62
VIII.	$ZnFe_2O_4$: Mohr's salt	1:5	425	21.94	78.06
IX.	$ZnFe_2O_4$: Mohr's salt	1:5	450	29.25	70.75
X.	$ZnFe_2O_4$: Amm-Fe(III) salt	1:5	400	38.06	61.94
XI.	$ZnFe_2O_4$: Amm-Fe(III) salt	1:5	425	35.26	64.74
XII.	$ZnFe_2O_4$: Amm-Fe(III) salt	1:5	450	46.076	53.93

Figures

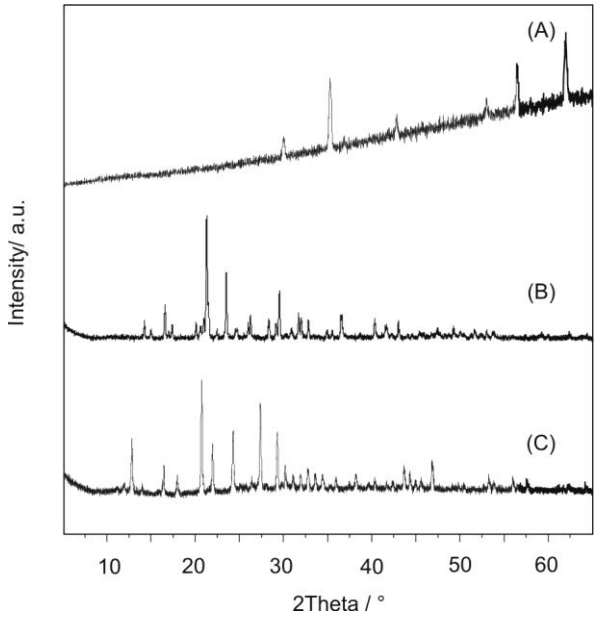

Figure 1. XRD patterns of (a) $ZnFe_2O_4$; (b) $(NH_4)_2Fe(SO_4)_2 \cdot 6H_2O$ and (c) $NH_4Fe(SO_4)_2 \cdot 12H_2O$

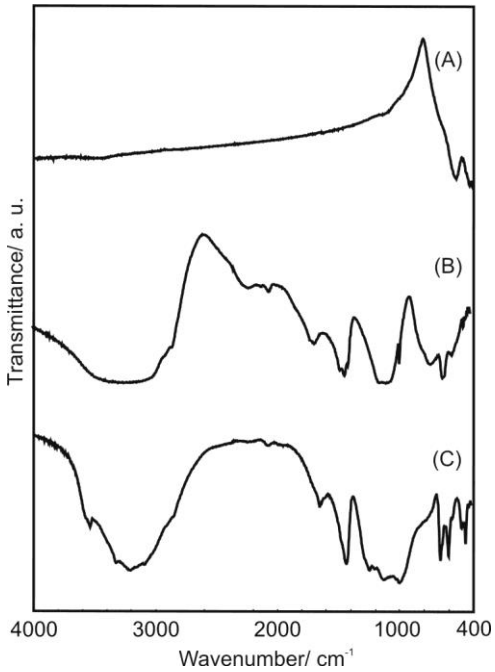

Figure 2. FTIR spectra of (a) $ZnFe_2O_4$; (b) $(NH_4)_2Fe(SO_4)_2 \cdot 6H_2O$ and (c) $NH_4Fe(SO_4)_2 \cdot 12H_2O$

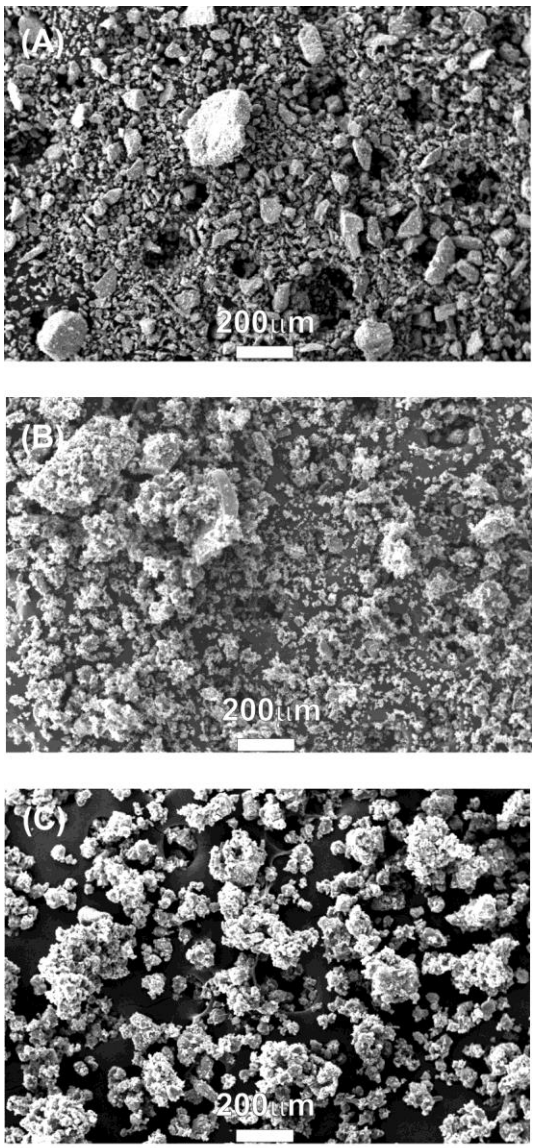

Figure 3. SEM images of (a) $ZnFe_2O_4$; (b) $(NH_4)_2Fe(SO_4)_2 \cdot 6H_2O$ and (c) $NH_4Fe(SO_4)_2 \cdot 12H_2O$

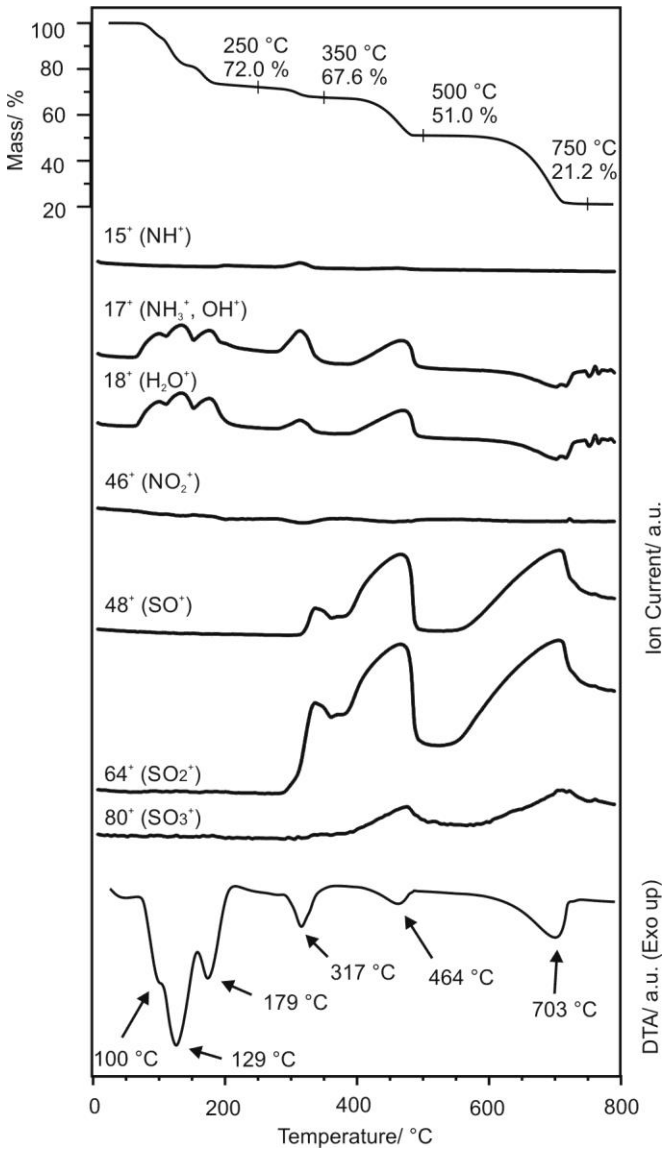

Fig. 4. TG/DTA and EGA-MS curves of $(NH_4)_2Fe(SO_4)_2 \cdot 6H_2O$ in air

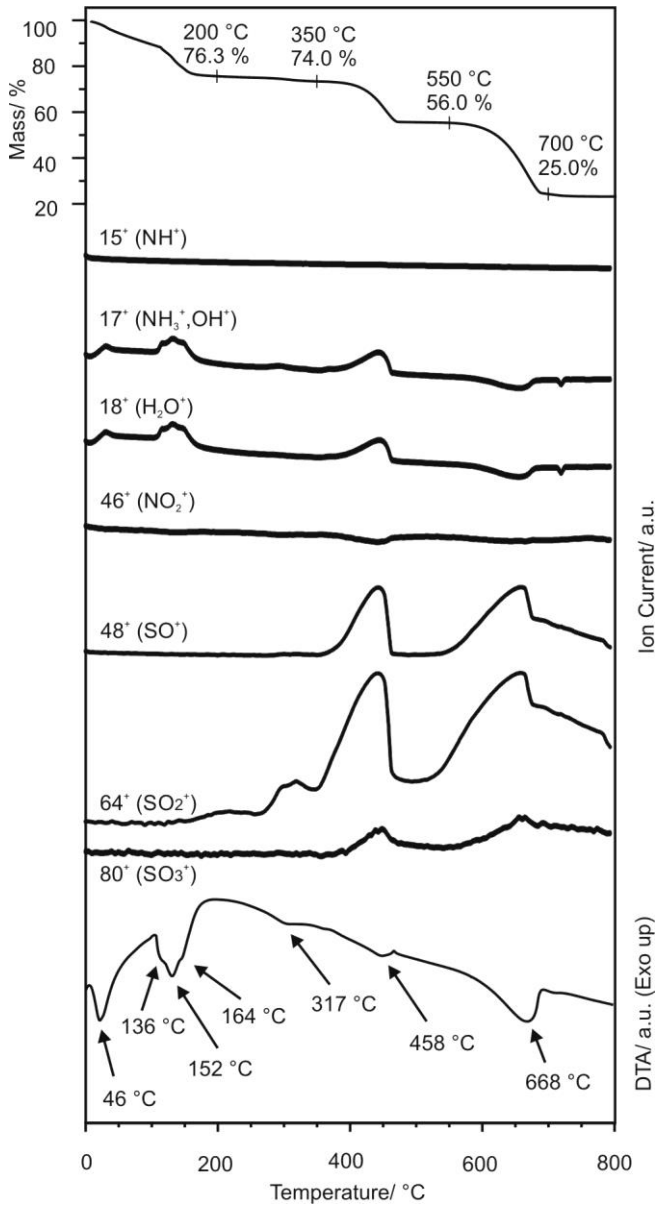

Fig. 5. TG/DTA and EGA-MS curves of $NH_4Fe(SO_4)_2 \cdot 12H_2O$ in air

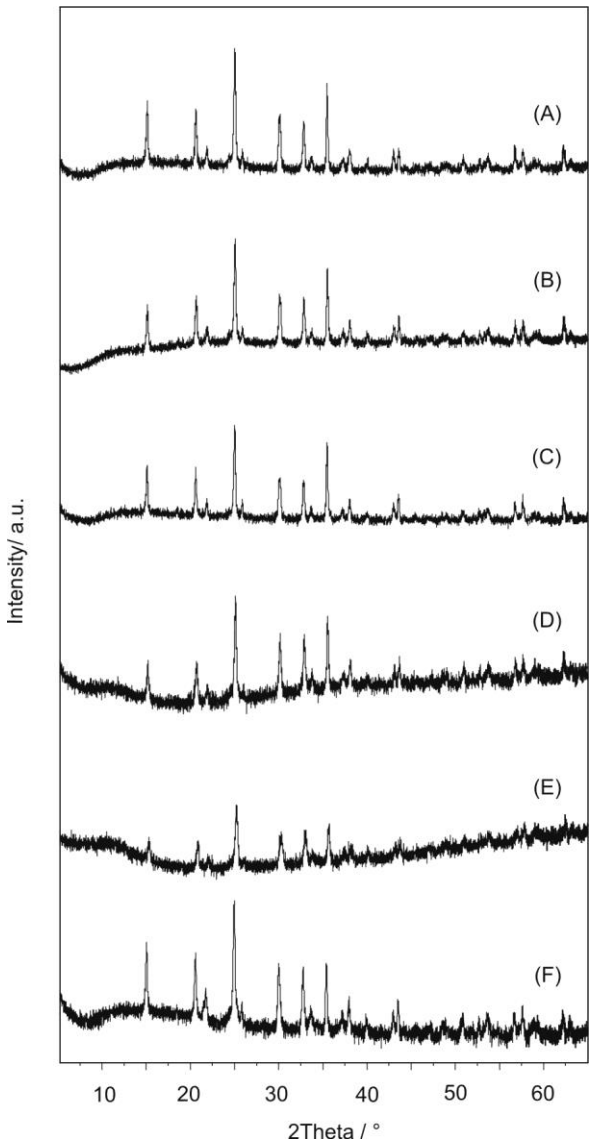

Fig. 6. XRD patterns of the 1:2 mixture of $ZnFe_2O_4$ and $(NH_4)_2Fe(SO_4)_2 \cdot 6H_2O$ annealed at (a) 400 °C; (b) 425 °C; (c) 450 °C and XRD patters of the 1:2 mixture of $ZnFe_2O_4$ and $NH_4Fe(SO_4)_2 \cdot 12H_2O$ annealed at (d) 400 °C; (e) 425 °C; (f) 450 °C

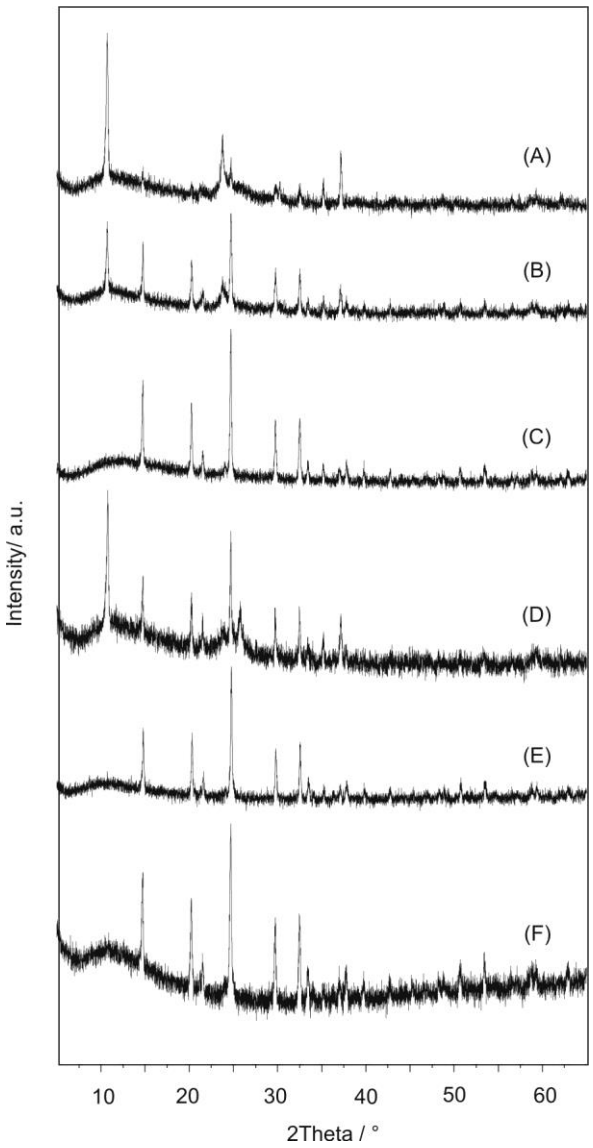

Fig. 7. XRD patterns of the 1:5 mixture of $ZnFe_2O_4$ and $(NH_4)_2Fe(SO_4)_2 \cdot 6H_2O$ annealed at (a) 400 °C; (b) 425 °C; (c) 450 °C and XRD patters of the 1:5 mixture of $ZnFe_2O_4$ and $NH_4Fe(SO_4)_2 \cdot 12H_2O$ annealed at (d) 400 °C; (e) 425 °C; (f) 450 °C

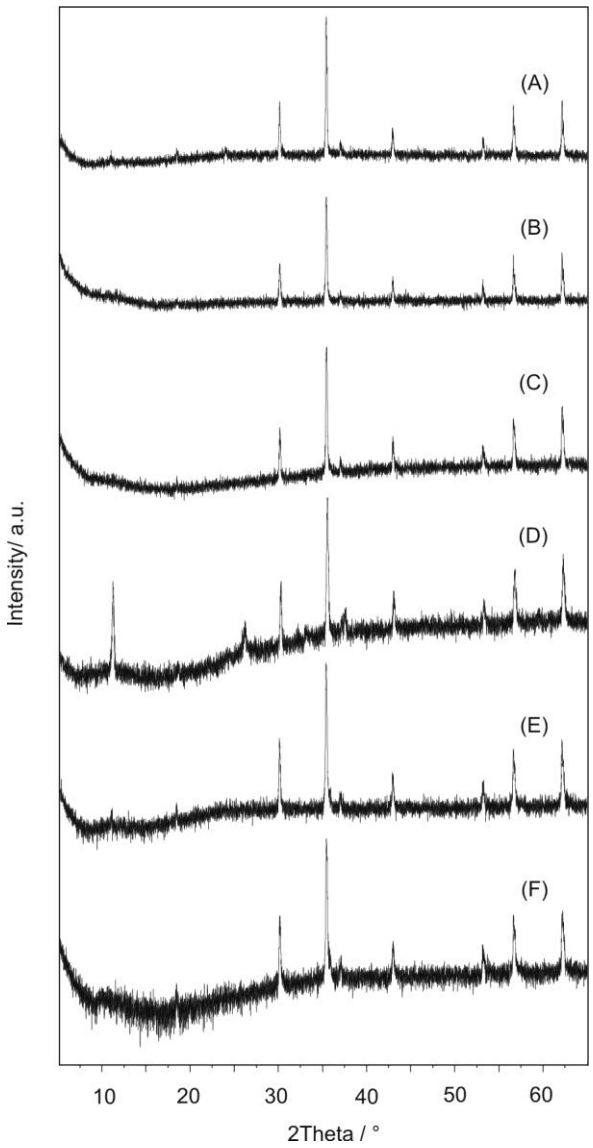

Fig. 8. XRD patterns after H_2O washing step of the 1:5 mixture of $ZnFe_2O_4$ and $(NH_4)_2Fe(SO_4)_2 \cdot 6H_2O$ annealed at (a) 400 °C; (b) 425 °C; (c) 450 °C and XRD patters of the 1:5 mixture of $ZnFe_2O_4$ and $NH_4Fe(SO_4)_2 \cdot 12H_2O$ annealed at (d) 400 °C; (e) 425 °C; (f) 450 °C

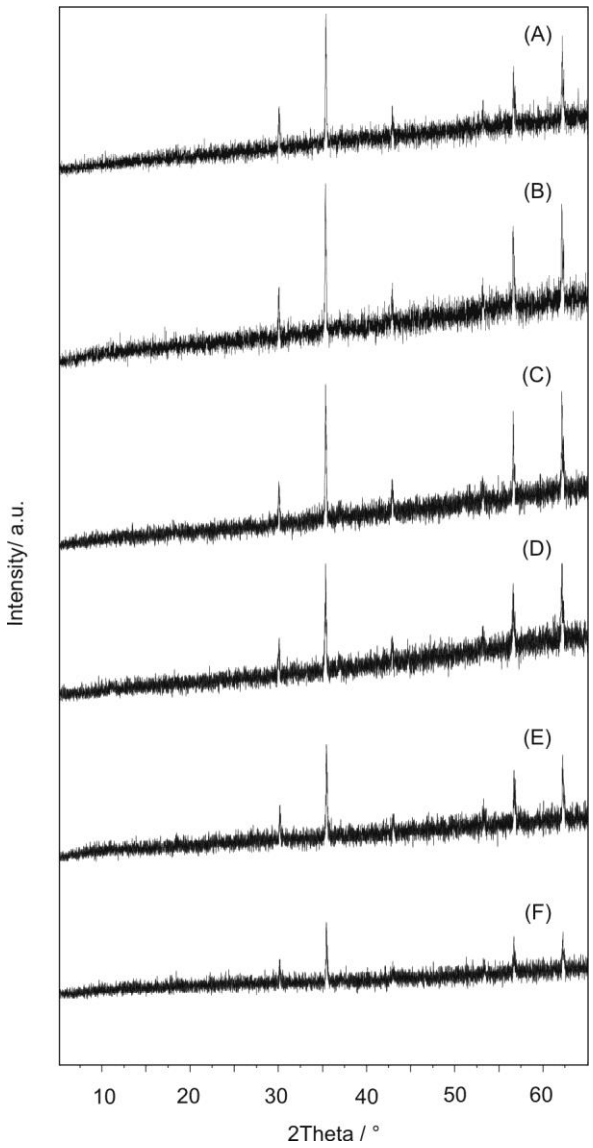

Fig. 9. XRD patterns after both H_2O and HCl washing steps of the 1:5 mixture of $ZnFe_2O_4$ and $(NH_4)_2Fe(SO_4)_2 \cdot 6H_2O$ annealed at (a) 400 °C; (b) 425 °C; (c) 450 °C and XRD patters of the 1:5 mixture of $ZnFe_2O_4$ and $NH_4Fe(SO_4)_2 \cdot 12H_2O$ annealed at (d) 400 °C; (e) 425 °C; (f) 450 °C

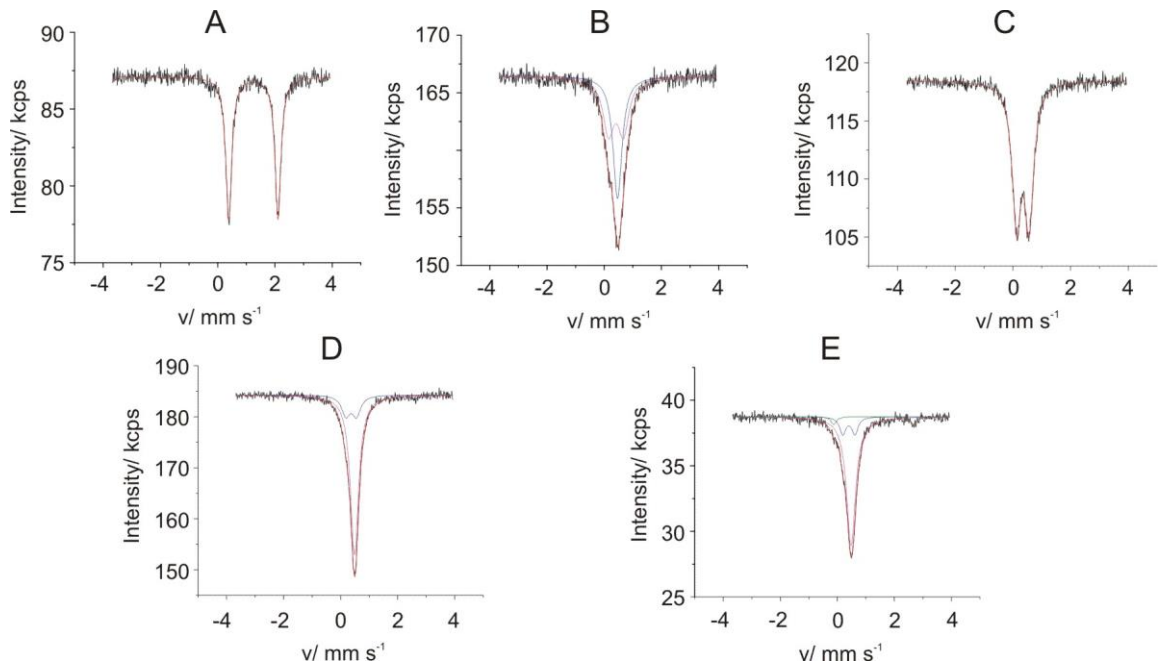

Fig. 10. Mössbauer spectra of (a) $(NH_4)_2Fe(SO_4)_2{\cdot}6H_2O$;(b) $NH_4Fe(SO_4)_2{\cdot}12H_2O$;(c) $ZnFe_2O_4$; (d) 1:5 mixture of $ZnFe_2O_4$ and $(NH_4)_2Fe(SO_4)_2{\cdot}6H_2O$ annealed 425 °C; and (e) 1:5 mixture of $ZnFe_2O_4$ and $NH_4Fe(SO_4)_2{\cdot}12H_2O$ annealed at 425 °C